

## HIV

# Lenacapavir treatment-emergent HIV-1 capsid resistance mutations are frequently associated with replication defects

Nina Pennetzdorfer<sup>1\*</sup>, Vidula Naik<sup>1</sup>, Sally Demirdjian<sup>1</sup>, Matthew R. Hendricks<sup>1</sup>, Cooper S. Jamieson<sup>2</sup>, Jason K. Perry<sup>2</sup>, Laurie A. VanderVeen<sup>1</sup>, Stephen R. Yant<sup>3</sup>, Hadas Dvory-Sobol<sup>4</sup>, Onyema Ogbuagu<sup>5</sup>, Samir K. Gupta<sup>6</sup>, Nicolas A. Margot<sup>1</sup>, Christian Callebaut<sup>1</sup>

Copyright © 2026 The Authors, some rights reserved; exclusive licensee American Association for the Advancement of Science. No claim to original U.S. Government Works

Lenacapavir (LEN) is a long-acting HIV-1 capsid inhibitor that binds to the HIV-1 capsid protein with picomolar antiviral activity, disrupting its function and inhibiting viral replication. Here, we identified capsid mutations in samples from individuals treated with LEN across two clinical trials that were considered potential LEN resistance-associated mutations. The *gag* encoding regions of clinical isolates with capsid mutations, as well as associated site-directed mutants, were cloned into the infectious molecular clone pXXLAI and pNL4-3-JRFL-secNLuc, encoding replication-competent HIV-1. Their effects on LEN susceptibility, replication kinetics, and three-dimensional capsid structure were investigated. Phenotypic analyses of the HIV-1 clinical isolates and site-directed mutants revealed that all resistance-associated mutations decreased LEN susceptibility to various degrees but were frequently associated with substantial replication defects. Structural modeling confirmed that LEN binding in the binding pocket was altered in the presence of capsid mutations, with predicted binding affinity changes correlating with observed potency shifts. These findings provide insights into LEN-resistance mechanisms and underscore the unusually high fitness costs associated with treatment-emergent capsid mutations.

## INTRODUCTION

Lenacapavir (LEN) is a multistage, antiretroviral inhibitor that selectively targets the HIV-1 capsid protein (1). LEN is approved as a stand-alone twice-yearly option for HIV-1 preexposure prophylaxis (PrEP) (2, 3) in the US and Europe and as a twice-yearly subcutaneous injectable in combination with other antiretrovirals for heavily treatment-experienced people with multidrug-resistant HIV-1 in several countries (4). LEN is also under investigation for maintenance of virologic suppression in treatment-experienced people living with HIV-1 (PLWH) in combination with other antiretrovirals.

The HIV capsid is a self-assembled cone-shaped structure composed of ~1500 capsid protein subunits, which include ~250 capsid protein hexamers and 12 capsid protein pentamers. This capsid shell protects the replicating viral genome as it infects new cells and travels to the nucleus. The arrangement and structure of the capsid protein are crucial for capsid stability and function during the viral infection cycle (5, 6). LEN binds to a well-defined pocket formed between adjacent subunits in capsid protein hexamers, disrupting early replication events before integration in part by decreasing capsid disassembly. In the later stages, LEN accelerates capsid assembly with structural alterations, leading to aberrant capsids and loss of viral infectivity (1, 7–9). LEN is a potent antiretroviral agent, exhibiting picomolar antiviral activity at both the early and late stages of the viral replication cycle [50% effective inhibitory concentration (EC<sub>50</sub>) for LEN = 30 to 100 pM at early stages]. LEN's intrinsic

metabolic and physicochemical properties, including slow-release kinetic and low aqueous solubility, have enabled the development of a subcutaneous formulation suitable for twice-yearly dosing (10, 11).

In heavily treatment-experienced individuals with multidrug-resistant HIV-1 infection, subcutaneous LEN combined with an optimized background regimen of antiretrovirals led to high rates of virological suppression and was well tolerated in a phase 2/3 trial (CAPELLA, NCT04150068) (12–14). Participants enrolled in this study had limited treatment options because of preexisting resistance to the four main classes of antiretrovirals [nucleoside reverse transcriptase (RT) inhibitors (NRTIs), non-nucleoside reverse transcriptase inhibitors (NNRTIs), protease inhibitors (PIs), and integrase strand-transfer inhibitors (INSTIs)]. Despite having extensive drug resistance and median HIV-1 RNA concentrations greater than 4 log<sub>10</sub> copies/ml, more than 81% of participants who received LEN plus an optimized background regimen achieved HIV-1 RNA below 50 copies/ml through week 104 of the study (15).

The CALIBRATE study (NCT04143594) was designed to generate clinical data on efficacy and safety of subcutaneous and oral LEN in combination with oral antiretroviral agents in treatment-naïve PLWH. Across the three cohorts receiving LEN in CALIBRATE, when missing data were excluded, virologic suppression was 98 to 100% at study week 80 (16). All participants enrolled in CAPELLA and CALIBRATE had wild-type (WT) phenotypic susceptibility to LEN at baseline (12, 16).

Resistance to LEN has been studied through in vitro resistance selection experiments, which identified amino acid substitutions L56I, M66I, Q67H, N74D, K70N, Q67H+N74S, and Q67H+T107N in the LEN binding pocket (1). In heavily treatment-experienced participants (CAPELLA), treatment-emergent capsid resistance occurred in 19% of participants (14 of 72) after 2 years, with variants including M66I, Q67H/K/N, K70H/N/R/S, N74D/H/K, A105T,

<sup>1</sup>Gilead Sciences, Clinical Virology, Foster City, CA 94404, USA. <sup>2</sup>Gilead Sciences, Structural Biology & Chemistry, Foster City, CA 94404, USA. <sup>3</sup>Gilead Sciences, Discovery Virology, Foster City, CA 94404, USA. <sup>4</sup>Gilead Sciences, Clinical Development, Foster City, CA 94404, USA. <sup>5</sup>Yale University School of Medicine, New Haven, CT 06520, USA. <sup>6</sup>Indiana University School of Medicine, Indianapolis, IN 46202, USA.

\*Corresponding author. Email: nina.pennetzdorfer@gilead.com

and T107A/C/N/S. In treatment-naïve participants receiving LEN (CALIBRATE), the main capsid resistance-associated mutations (RAMs) observed were Q67H and K70R (in 2.2% of participants, 4 of 182) (16). The presence of these main capsid resistant variants observed in both studies was associated with reduced susceptibility to LEN, ranging from 4.5 to more than 869-fold relative to WT control virus (14).

Here, we present data on the interactions between LEN and capsid RAMs at the molecular stage. We provide a comprehensive phenotypic and structural characterization of LEN resistance using clinical isolates and site-directed mutants (SDMs) from the CAPELLA and CALIBRATE studies in single-cycle and multicycle HIV-1 inhibition assays. This study provides mechanistic insights into the effective use of LEN in support of ongoing efforts to combat the HIV-1 pandemic.

## RESULTS

### Comprehensive assessment of LEN susceptibility of capsid resistance mutations

To evaluate the impact of capsid RAMs on the antiviral activity of LEN, we tested 40 HIV-1 clinical isolates and 44 SDMs using three complementary phenotypic assays: the 2-day single-cycle PhenoSense Gag-Pro reporter assay, the 5-day multicycle MT-2 cytopathic assay, and the 5-day multicycle RevLun antiviral reporter assay. All constructs were subcloned into the infectious molecular clone pXXLAI (subtype B), encoding the complete gag regions from both treatment-naïve and heavily treatment-experienced clinical samples (in total 40 clinical isolates; table S1, nos. 1 to 40). Mutations found in the clinical isolates were further assessed by introducing these capsid RAMs into the gag gene of pXXLAI by site-directed mutagenesis (in total 44 SDM constructs, table S1, nos. 41 to 84) to investigate the effects of individual and combined capsid RAMs observed clinically.

LEN EC<sub>50</sub> fold change data ranged from values comparable to those of WT to increases exceeding 2500-fold. To ensure interpretability, resistance categories were defined as follows: no resistance (0- to 3.5-fold), low resistance (>3.5- to 25-fold), medium resistance (>25- to 100-fold), and high resistance (>100-fold). The range of the “no resistance” category was based on the LEN fold change observed in clinical baseline samples before capsid RAM emergence, indicating that values in this range reflect WT susceptibility (fig. S1). Subsequent thresholds were chosen to provide distinct separation between minor, moderate, and substantial shifts in LEN susceptibility. These thresholds are used consistently throughout the Results section and are illustrated in Fig. 1 and Table 1. Each data point reflects the average fold change relative to WT from at least three independent experimental replicates (fig. S2 and table S1).

The Q67H+K70R group represented a distinct resistance pathway and was frequently observed in clinical isolates (Fig. 1, Table 1, fig. S2, and table S1). Single substitutions at these positions conferred only modest resistance: Q67H alone typically resulted in low resistance with fold change values between 4.7- and 13.8-fold, whereas K70R alone had susceptibility similar to WT (LEN-resistance fold change of 0.8). In contrast, the Q67H+K70R double mutant produced an increase in resistance, with median fold change values at 28.6 and interquartile range (IQR) extending up to 37.4, placing it in the medium resistance category. The addition of further substitutions, such as A105T or T107N, further amplified resistance to the

medium and high ranges, respectively. Although Q67H and K70R individually exert limited resistance effects, their combination created a potentially synergistic disruption of the LEN binding pocket; accessory mutations seemed to further destabilize the capsid interface to drive resistance.

Among the resistance mutations evaluated, M66I was the most frequent and consistently conferred high resistance to LEN (Fig. 1, Table 1, fig. S2, and table S1). In the RevLun assay, M66I alone resulted in fold change values well above 100-fold, and when combined with additional substitutions such as Q67H, N74D, A105T, or T107S, LEN susceptibility frequently exceeded the highest concentration tested (100 nM, fold change > 1000). These combinations were associated with reduced infectivity in the MT-2 assay, limiting their characterization in that system. However, the RevLun assay enabled robust phenotyping of these variants, confirming their resistance profiles despite low cytopathic effect in MT-2 assays (fig. S2 and table S1).

LEN susceptibility varied across other mutation combinations, depending on their genetic context. Single mutations such as N74D or T107N generally conferred low-to-medium resistance. However, when these mutations were combined with Q67H±K70R, the resistance magnitude increased nonlinearly. For example, Q67H+N74D, Q67H+N74D+A105T, and Q67H+K70R+T107N all resulted in high LEN resistance. This suggests that certain RAM combinations may act synergistically to destabilize the capsid structure in a manner that substantially impairs LEN binding. The K70N+N74K and Q67K+K70H combinations also resulted in high resistance in the RevLun assay, although their infectivity was often compromised in the MT-2 assay, indicating a trade-off between resistance and fitness (Fig. 1, fig. S2, and table S1).

The RevLun assay proved essential for characterizing variants with reduced cytopathic effect, enabling phenotyping of 88% of the constructs. It confirmed susceptibility data for key variants and provided data for combinations of LEN RAMs that were otherwise non-infectious in the MT-2 assay. Together, data from all three assays provide a comprehensive overview of LEN susceptibility across the capsid resistance landscape and support the classification of distinct mutational pathways with varying resistance profiles and cooperativity between RAMs.

Strong correlations from linear regression analyses were observed across the assays for both baseline samples and capsid mutants (Fig. 2). In all three assays, baseline samples exhibited phenotypic susceptibility to LEN near WT ranges. LEN susceptibility measured in the Gag-Pro assay strongly correlated with the MT-2 assay results [Fig. 2A; correlation coefficient ( $r^2$ ) = 0.9012]. Similarly, susceptibility measured in the RevLun assay correlated highly with both the MT-2 assay (Fig. 2B;  $r^2$  = 0.7949) and the Gag-Pro assay (Fig. 2C;  $r^2$  = 0.8887).

### Replication kinetics of capsid mutants varied across the major resistance groups

Replication kinetics were assessed for all clinical isolates using a 14-day multicycle human peripheral blood mononuclear cell (PBMC) virus outgrowth assay in the absence of drug (Table 2 and fig. S3). The replication capacity was calculated by comparing the viral growth of variants on day 10 postinfection with that of the laboratory reference WT virus (NL4-3-JRFL-secNLuc). All 18 baseline clinical isolates exhibited replication capacity values >75% relative to WT, confirming robust replication before the emergence of capsid resistance mutations. Of note, no clinically

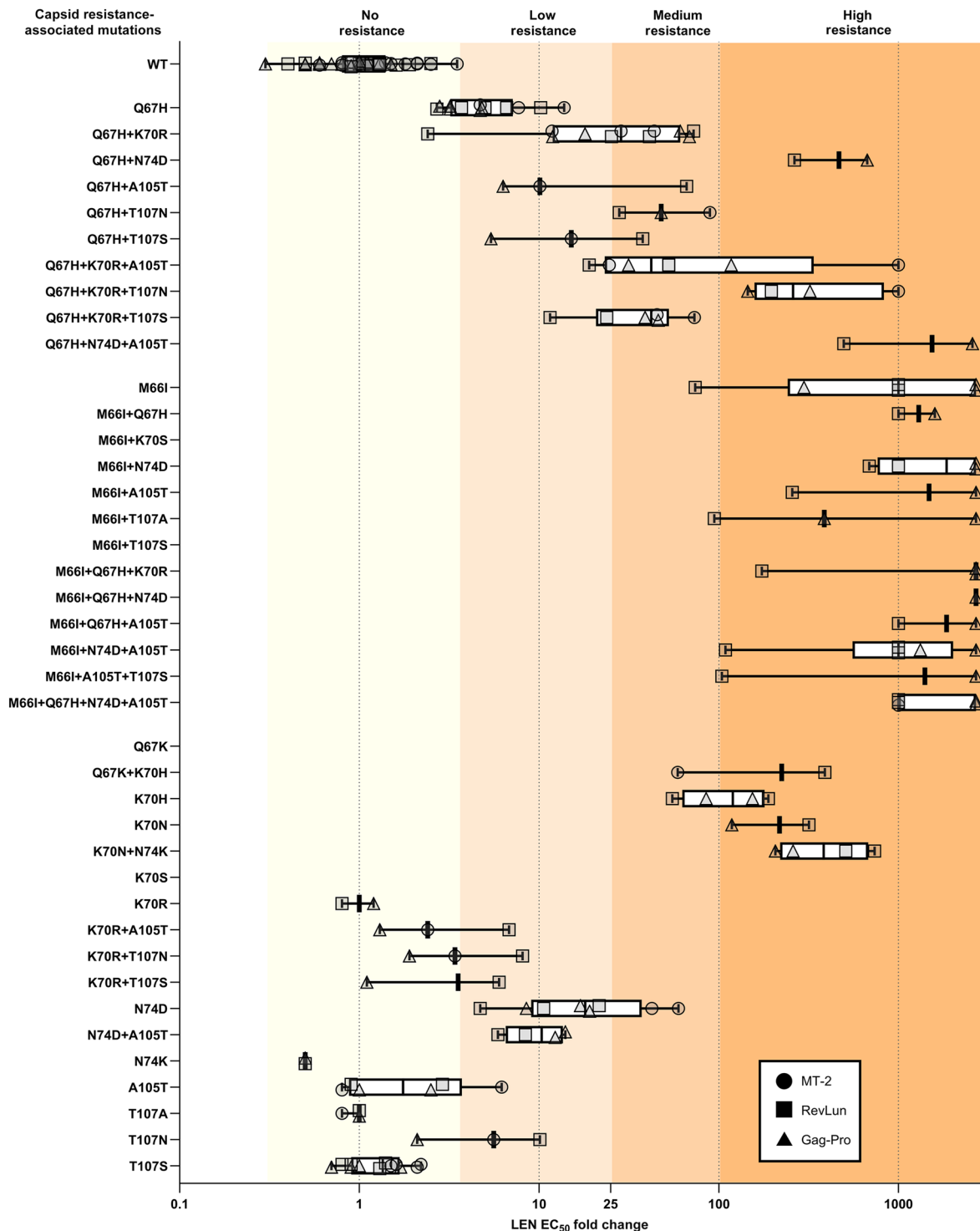


**Fig. 1. LEN EC<sub>50</sub> fold changes varied across capsid resistance mutations.** LEN susceptibility was tested in three phenotypic assays: the multicycle MT-2 (circles), multi-cycle RevLun (squares), and the single-cycle PhenoSense Gag-Pro assay (triangles). The range of LEN fold change values was normalized relative to the WT control [XXLAI for multicycle assays or drug-sensitive reference strain (CNDO) containing PR and RT sequences from HIV-1 strain NL4-3 for single-cycle assay]. This was plotted for all capsid mutations derived from clinical isolates as well as site-directed capsid mutants determined in the respective assay from at least three independent experiments, each performed in triplicate. Each box represents the IQR, with the vertical line indicating the median of all EC<sub>50</sub> fold change values derived from clinical isolates and SDM viruses across the three assays. Whiskers extend to the smallest and largest values within 1.5× IQR from the lower and upper quartiles, respectively. Box width does not reflect the sample size. Background shading denotes resistance categories: no resistance (0- to 3.5-fold), low resistance (3.5- to 25-fold), medium resistance (25- to 100-fold), and high resistance (>100-fold).

Downloaded from <https://www.science.org> on January 12, 2026

**Table 1. Summary of LEN EC<sub>50</sub> fold changes across capsid resistance mutations.** Median, IQR, minimum, and maximum EC<sub>50</sub> fold change values are shown, derived from clinical isolates and site-directed mutants across three phenotypic assays. Each data point contributing to the median reflects the average fold change relative to the WT virus [XXLAI for multicycle assays or drug-sensitive reference strain (CNDO) containing PR (protease) and RT sequences from HIV-1 strain NL4-3 for single-cycle assay] from at least three independent experimental replicates each performed in triplicate. NI, noninfectious.

| LEN-resistance mutation | LEN EC <sub>50</sub> fold change from WT |        |         |         | n of data points | n of constructs <sup>*</sup> |
|-------------------------|--|--------|---------|---------|------------------|------------------------------|
|                         | Median                                   | IQR    | Minimum | Maximum |                  |                              |
| WT/Baseline             | 1.0                                      | 0.6    | 0.3     | 3.5     | 43               | 16                           |
| Q67H                    | 4.7                                      | 3.4    | 2.7     | 13.8    | 13               | 5                            |
| Q67H+K70R               | 28.6                                     | 37.4   | 2.4     | 72.5    | 11               | 4                            |
| Q67H+N74D               | 467.0                                    | 203.6  | 263.4   | 670.5   | 2                | 1                            |
| Q67H+A105T              | 10.1                                     | 30.0   | 6.3     | 66.3    | 3                | 1                            |
| Q67H+T107N              | 47.8                                     | 30.7   | 27.9    | 89.2    | 3                | 1                            |
| Q67H+T107S              | 15.1                                     | 16.2   | 5.4     | 37.7    | 3                | 1                            |
| Q67H+K70R+A105T         | 42.1                                     | 74.8   | 19.0    | 1000.0  | 6                | 2                            |
| Q67H+K70R+T107N         | 259.0                                    | 308.0  | 145.0   | 1000.0  | 4                | 2                            |
| Q67H+K70R+T107S         | 42.1                                     | 18.3   | 11.5    | 73.2    | 6                | 2                            |
| Q67H+N74D+A105T         | 1536.7                                   | 1041.4 | 495.3   | 2578.1  | 2                | 1                            |
| M66I                    | 1000.0                                   | 1801.5 | 74.0    | 2700.0  | 6                | 3                            |
| M66I+Q67H               | 1297.0                                   | 297.0  | 1000.0  | 1594.0  | 2                | 1                            |
| M66I+K70S               | NI                                       | NI     | NI      | NI      | NI               | 2                            |
| M66I+N74D               | 1850.0                                   | 1778.3 | 686.7   | 2700.0  | 4                | 2                            |
| M66I+A105T              | 1478.1                                   | 1222.0 | 256.1   | 2700.0  | 2                | 1                            |
| M66I+T107A              | 386.3                                    | 1302.9 | 94.3    | 2700.0  | 3                | 2                            |
| M66I+T107S              | NI                                       | NI     | NI      | NI      | NI               | 1                            |
| M66I+Q67H+K70R          | 2700.0                                   | 1263.3 | 173.5   | 2700.0  | 3                | 2                            |
| M66I+Q67H+N74D          | 2700.0                                   | 0.0    | 2700.0  | 2700.0  | 1                | 1                            |
| M66I+Q67H+A105T         | 1850.0                                   | 850.0  | 1000.0  | 2700.0  | 2                | 1                            |
| M66I+N74D+A105T         | 1000.0                                   | 324.0  | 109.0   | 2700.0  | 3                | 3                            |
| M66I+A105T+T107S        | 1402.1                                   | 1298.0 | 104.1   | 2700.0  | 2                | 1                            |
| M66I+Q67H+N74D+A105T    | 1000.0                                   | 1700.0 | 1000.0  | 2700.0  | 5                | 2                            |
| Q67K                    | NI                                       | NI     | NI      | NI      | NI               | 1                            |
| Q67K+K70H               | 224.1                                    | 165.1  | 59.0    | 389.2   | 2                | 2                            |
| K70H                    | 119.5                                    | 85.1   | 55.2    | 188.7   | 4                | 2                            |
| K70N                    | 217.8                                    | 99.8   | 118.0   | 317.6   | 2                | 1                            |
| K70N+N74K               | 383.6                                    | 319.2  | 206.2   | 735.5   | 4                | 2                            |
| K70S                    | NI                                       | NI     | NI      | NI      | NI               | 1                            |
| K70R                    | 1.0                                      | 0.2    | 0.8     | 1.2     | 2                | 1                            |
| K70R+A105T              | 2.4                                      | 2.8    | 1.3     | 6.8     | 3                | 1                            |
| K70R+T107N              | 3.4                                      | 3.1    | 1.9     | 8.1     | 3                | 1                            |
| K70R+T107S              | 3.6                                      | 2.5    | 1.1     | 6.0     | 2                | 1                            |
| N74D                    | 18.1                                     | 16.7   | 4.7     | 59.7    | 8                | 3                            |
| N74D+A105T              | 10.4                                     | 5.0    | 5.9     | 14.0    | 4                | 2                            |
| N74K                    | 0.5                                      | 0.0    | 0.5     | 0.5     | 2                | 1                            |
| A105T                   | 1.8                                      | 1.9    | 0.8     | 6.2     | 6                | 2                            |
| T107A                   | 1.0                                      | 0.1    | 0.8     | 1.0     | 3                | 1                            |
| T107N                   | 5.6                                      | 4.0    | 2.1     | 10.1    | 3                | 1                            |
| T107S                   | 1.4                                      | 0.7    | 0.7     | 2.2     | 12               | 4                            |

\*Total number of constructs was 84 (40 clinical isolates and 44 site-directed mutants).

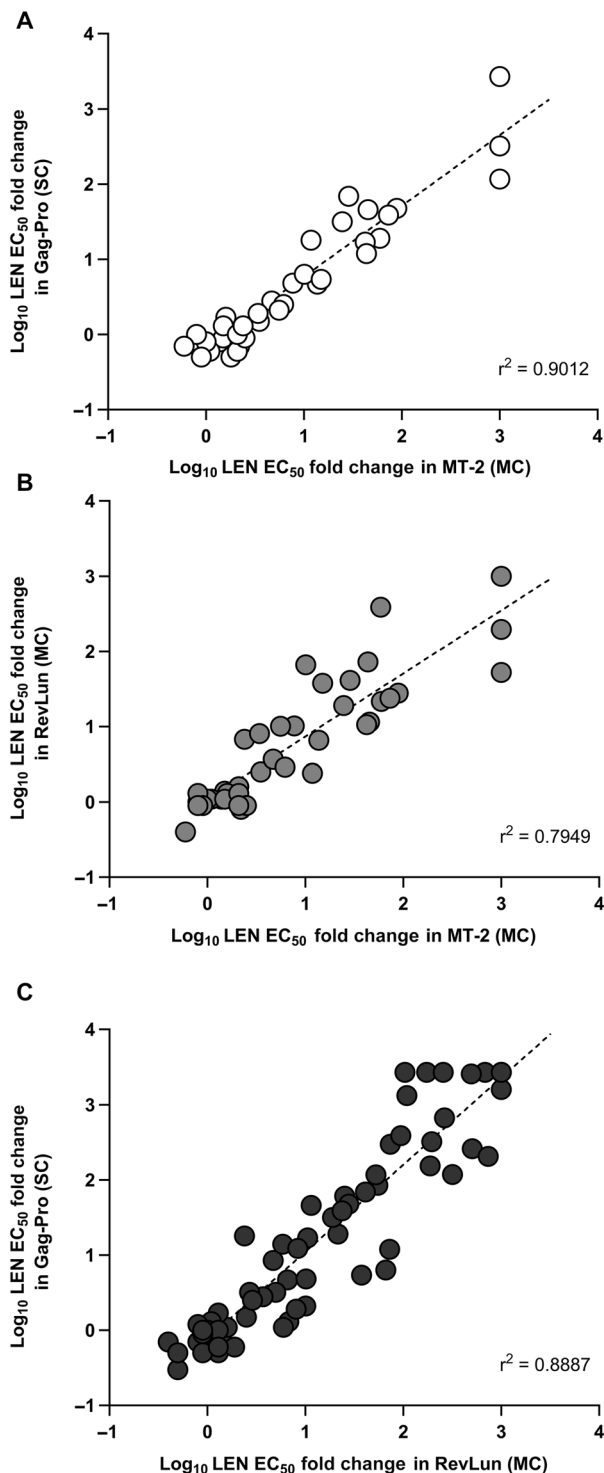


**Fig. 2. LEN susceptibility of clinical isolates and SDMs was consistent across assays.** Changes in susceptibility to LEN obtained in different assays for the mutants tested are plotted and were analyzed by linear regression. The dashed lines represent the respective regression lines. (A to C) Comparisons of single-cycle PhenoSense Gag-Pro assay versus multicycle MT-2 assay (A), multicycle RevLun assay versus multicycle MT-2 assay (B), and multicycle RevLun assay versus single-cycle PhenoSense Gag-Pro assay (C) are shown along with the corresponding  $r^2$ . SC, single-cycle; MC, multicycle.

validated replication capacity cutoff currently exists; therefore, replication capacity values should be interpreted in the context of the overall treatment regimen rather than as an isolated predictor of clinical outcome.

Distinct replication kinetic patterns emerged across the major resistance groups. Variants containing M66I±A105T±T107A/S showed the greatest impairment, with replication capacity values ranging between 13 and 17% of WT, indicating that M66I imposes a substantial fitness cost (Table 2 and fig. S3). Partial restoration of replication capacity was observed upon the addition of N74D and A105T to M66I (mean of 40% replication capacity). Replication capacity was further improved with the addition of Q67H to ranges comparable to those seen for resistance mutations in other drug classes (NRTI, NNRTI, PI, and INSTI classes; fig. S4 and table S2). In contrast, viruses with Q67H alone were mostly fit with an average replication capacity of 63% of WT, ranging from 94 to 22.7%, indicating that the sequence context across these three mutants may affect replication capacity differentially. Similarly, the Q67H+K70R double mutant was associated with >75% of WT replication in all but one sample (33% for sample 38) (Table 2 and fig. S3). Other single mutations, such as N74D or K70H, resulted in replication capacity reductions to 28% of WT. The double mutation K70N+N74K ranked similarly at 24% of WT, whereas the addition of Q67K to K70H restored viral fitness from 28 to 98% of WT. These observations show that some resistance mutation groups have limited impact on viral replication, whereas others, particularly M66I single mutations, result in marked impairment.

To contextualize the replication capacity of capsid mutants, we evaluated representative RAMs from other antiretroviral drug classes using the same multicycle PBMC-based system. SDMs harboring RT, IN, or PR mutations were introduced into the NL4-3-JRFL-secNLuc backbone and assessed over 14 days (fig. S4 and table S2). RT mutations associated with NRTI resistance (K65R and M184V) showed moderate reductions in replication capacity values (66 and 75% of WT, respectively), whereas NNRTI resistance mutations (K103N and Y181C) retained higher replication capacity values (83 and 79% of WT, respectively). INSTI resistance mutations (N155H and R263K) exhibited minimal impact on replication capacity (82 and 85% of WT, respectively). The I50L PI resistance mutation had a moderate effect on replication capacity (66% of WT), whereas the I50V mutant showed a more pronounced replication capacity impairment (23% of WT). These data highlight that replication deficits observed for certain capsid mutants are frequently more severe than those seen with resistance mutations in other antiretroviral classes.

We observed a trend of an inverse relationship between replication capacity of clinical isolates in PBMCs and their reduction in LEN susceptibility observed in the RevLun assay (Fig. 3A). We also evaluated the replication capacity of all constructs in the single-cycle PhenoSense Gag-Pro assay, comparing viral growth with that of WT in the absence of drug. Most viruses with capsid mutations tested in the Gag-Pro assay exhibited a decrease in replication capacity that similarly coincided with a decrease in LEN susceptibility, including M66I and N74D (replication capacity < 30% of WT, Table 1; Fig. 3B). Overall, the single-cycle data were consistent with the findings in the multicycle PBMC assay and indicate that the replication capacity of most M66I-containing LEN-selected capsid RAMs is compromised.

**Table 2. Replication capacity of HIV-1 variants with LEN-resistance mutations.** The subcloned Gag and PR coding regions derived from baseline samples from respective participants who developed capsid RAMs and the subcloned *gag-pro* fragments encoding resistance mutations of each participant are listed. The replication capacity is expressed as the percentage of WT control [drug-sensitive reference strain (CNDO) containing PR and RT sequences from HIV-1 strain NL4-3 in the Gag-Pro single cycle assay and laboratory strain NL4-3 in the multicycle PBMC assay]. The multicycle PBMC data were replicated at least three times individually with four technical replicates per time point. The table is sorted from highest to lowest PBMC replication capacity values to highlight the impact of specific mutation combinations on viral fitness. Dashes indicate no LEN-resistance mutation. AF, assay failure; CI, clinical isolate; NA, not available; W, study week.

| Sample ID/HIV-1 subtype | Virus # | Visit/SDM | Source | LEN-resistance mutations |     |     |     |      |      | Summary              | Replication capacity  |                  |
|-------------------------|---------|-----------|--------|--------------------------|-----|-----|-----|------|------|----------------------|-----------------------|------------------|
|                         |         |           |        | M66                      | Q67 | K70 | N74 | A105 | T107 |                      | Gag-Pro single cycle* | PBMC multicycle† |
| 17 / B                  | 37      | Baseline  | CI     | -                        | -   | -   | -   | -    | -    | None                 | 78.0                  | 131.0            |
| 10 / B                  | 21      | Baseline  | CI     | -                        | -   | -   | -   | -    | -    | None                 | 74.0                  | 112.9            |
| 8 / B                   | 17      | Baseline  | CI     | -                        | -   | -   | -   | -    | -    | None                 | 146.0                 | 109.9            |
| 12 / B                  | 27      | Baseline  | CI     | -                        | -   | -   | -   | -    | S    | T107S                | 101.0                 | 109.2            |
| 1 / B                   | 1       | Baseline  | CI     | -                        | -   | -   | -   | -    | -    | None                 | 93.0                  | 104.3            |
| 7 / B                   | 15      | Baseline  | CI     | -                        | -   | -   | -   | -    | S    | T107S                | 293.0                 | 101.7            |
| 5 / BF                  | 12      | W52       | CI     | -                        | K   | H   | -   | -    | -    | Q67K+K70H            | 88.0                  | 98.0             |
| 3 / AE                  | 6       | Baseline  | CI     | -                        | -   | -   | -   | -    | -    | None                 | 8.5                   | 95.8             |
| 13 / B                  | 29      | Baseline  | CI     | -                        | -   | -   | -   | -    | -    | None                 | 131.0                 | 95.1             |
| 6 / B                   | 13      | Baseline  | CI     | -                        | -   | -   | -   | -    | -    | None                 | 103.0                 | 94.8             |
| 5 / BF                  | 10      | Baseline  | CI     | -                        | -   | -   | -   | -    | -    | None                 | 98.0                  | 94.2             |
| 18 / B                  | 40      | W116      | CI     | -                        | H   | -   | -   | -    | -    | Q67H                 | 51.0                  | 94.0             |
| 15 / B                  | 33      | Baseline  | CI     | -                        | -   | -   | -   | -    | -    | None                 | 93.0                  | 92.6             |
| 9 / B                   | 19      | Baseline  | CI     | -                        | -   | -   | -   | -    | -    | None                 | 163.0                 | 91.1             |
| 11 / B                  | 26      | W130      | CI     | -                        | H   | R   | -   | -    | N    | Q67H+K70R+T107N      | 0.5                   | 89.7             |
| 8 / B                   | 18      | W10       | CI     | -                        | H   | R   | -   | -    | -    | Q67H+K70R            | 63.0                  | 89.3             |
| 16 / C                  | 35      | Baseline  | CI     | -                        | -   | -   | -   | -    | -    | None                 | 33.0                  | 88.5             |
| 11 / B                  | 24      | Baseline  | CI     | -                        | -   | -   | -   | -    | -    | None                 | 17.0                  | 85.8             |
| 4 / B                   | 8       | Baseline  | CI     | -                        | -   | -   | -   | -    | -    | None                 | 22.0                  | 82.7             |
| 18 / B                  | 39      | Baseline  | CI     | -                        | -   | -   | -   | -    | -    | None                 | 82.0                  | 80.0             |
| 7 / B                   | 16      | W4        | CI     | -                        | H   | R   | -   | -    | S    | Q67H+K70R+T107S      | 109.0                 | 79.2             |
| 2 / B                   | 4       | Baseline  | CI     | -                        | -   | -   | -   | -    | S    | T107S                | 10.0                  | 78.2             |
| 15 / B                  | 34      | W62       | CI     | -                        | H   | R   | -   | -    | -    | Q67H+K70R            | 19.0                  | 76.4             |
| 14 / AE                 | 31      | Baseline  | CI     | -                        | -   | -   | -   | -    | -    | None                 | 0.7                   | 75.1             |
| 9 / B                   | 20      | W54       | CI     | -                        | H   | -   | -   | -    | -    | Q67H                 | 49.0                  | 71.0             |
| 10 / B                  | 23      | W22       | CI     | I                        | H   | -   | D   | T    | -    | M66I+Q67H+N74D+A105T | 13.0                  | 64.2             |
| 10 / B                  | 22      | W10       | CI     | I                        | -   | -   | D   | T    | -    | M66I+N74D+A105T      | 16.0                  | 46.6             |
| 1 / B                   | 3       | W52-R     | CI     | I                        | -   | -   | D   | T    | -    | M66I+N74D+A105T      | 30.0                  | 34.2             |
| 17 / B                  | 38      | W80       | CI     | -                        | H   | R   | -   | -    | -    | Q67H+K70R            | 31.0                  | 33.0             |
| 14 / AE                 | 32      | W62       | CI     | -                        | -   | -   | D   | -    | -    | N74D                 | 1.0                   | 28.5             |
| 5 / BF                  | 11      | W10       | CI     | -                        | -   | H   | -   | -    | -    | K70H                 | 37.0                  | 28.0             |
| 4 / B                   | 9       | W4        | CI     | I                        | H   | R   | -   | -    | -    | M66I+Q67H+K70R       | 3.1                   | 24.8             |
| 16 / C                  | 36      | W52       | CI     | -                        | H   | -   | -   | -    | -    | Q67H                 | 9.6                   | 22.7             |
| 13 / B                  | 30      | W78       | CI     | -                        | -   | N   | K   | -    | -    | K70N+N74K            | 55.0                  | 19.6             |
| 1 / B                   | 2       | W26/52    | CI     | I                        | -   | -   | -   | -    | -    | M66I                 | 12.0                  | 17.1             |
| 2 / B                   | 5       | W26/52    | CI     | I                        | -   | -   | -   | T    | S    | M66I+A105T+T107S     | 1.2                   | 16.7             |
| 6 / B                   | 14      | W4        | CI     | I                        | -   | -   | -   | -    | A    | M66I+T107A           | 24.0                  | 15.4             |
| 12 / B                  | 28      | W88       | CI     | -                        | H   | R   | -   | T    | -    | Q67H+K70R+A105T      | 122.0                 | NA               |
| 11 / B                  | 25      | W88       | CI     | -                        | H   | -   | -   | -    | -    | Q67H                 | 70.0                  | NA               |
| 3 / AE                  | 7       | W4        | CI     | I                        | -   | S   | -   | -    | -    | M66I+K70S            | AF                    | NA               |

\*Single-cycle replication capacity expressed as % of WT control [drug-sensitive reference strain (CNDO) containing PR and RT sequences from HIV-1 and NL4-3]. †Multicycle replication capacity expressed as % WT control (NL4-3 containing Gag and PR encoding region from the LAI reference strain) in human PBMCs at day 10; values represent the mean of at least three independent replicate experiments.

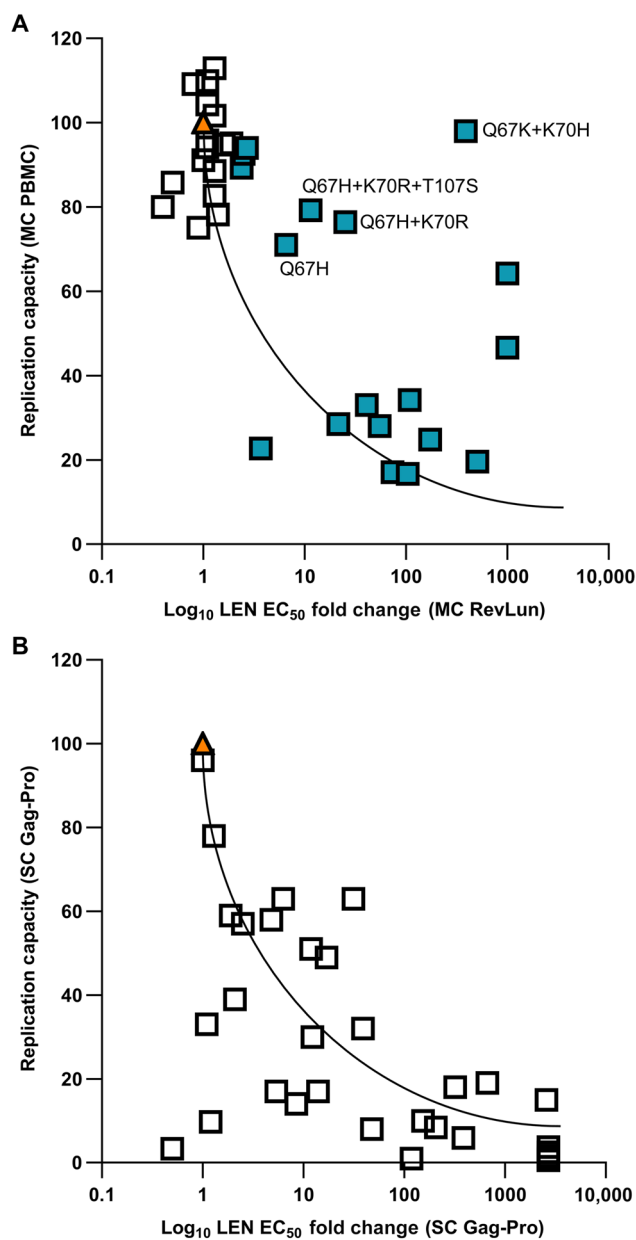


**Fig. 3. Reduced replication capacity frequently coincided with LEN resistance.**

The replication capacity of the WT virus reference standard was set at 100%, and the replication capacity values of the mutant viruses were calculated as a percentage of this value. The WT capsid is highlighted as an orange triangle. **(A)** Comparisons of replication capacity from clinical isolates obtained in multicycle PBMC assay versus multicycle RevLun phenotyping assay are shown. Replication capacity was assessed in a 14-day viral outgrowth kinetics experiment in human PBMCs and expressed relative to the WT virus (NL4-3-JRFL-secNLuc). Postbaseline samples are highlighted in teal. Clinical isolates with preserved replication capacity despite a higher LEN EC<sub>50</sub> fold change value are highlighted. **(B)** Comparisons of replication capacity from SDMs obtained in single-cycle PhenoSense Gag-Pro assay versus fold change in the single-cycle PhenoSense Gag-Pro assay are displayed. Replication capacity is expressed as the percentage of WT control [drug-sensitive reference strain (CNDO) containing protease and reverse transcriptase sequences from HIV-1 strain NL4-3].

### FEP predictions and structural analyses indicate capsid mutations disrupt LEN binding via hydrophobic and hydrogen bond changes

To quantitatively assess the impact of capsid mutations on LEN binding affinity, free energy perturbation (FEP) calculations were performed on 38 LEN:capsid protein mutant complexes. Simulations showed moderate correlation with experimental fold change values (Kendall's Tau = 0.65; Fig. 4 and table S3). Predictions deviated from experimental observations (>2 kcal/mol) when mutations altered side-chain charge, such as K70N and N74D (48 and 50 in Fig. 4, respectively). Despite LEN's complex mode of action and variable viral fitness, the moderate correlation between predicted and experimental EC<sub>50</sub> fold change values supported FEP as a reasonable predictor of mutational effects on LEN binding affinity.

On the basis of the x-ray crystal structure of LEN bound to a cross-linked capsid protein hexamer (Fig. 5A) (I), the LEN binding pocket was primarily formed between the N-terminal domain (NTD) of one subunit (CA-1) and the C-terminal domain (CTD) of another [CA-2; (I, 8)]. We found that clinically observed LEN RAMs were associated with CA-1. M66 shaped the hydrophobic pocket for LEN's

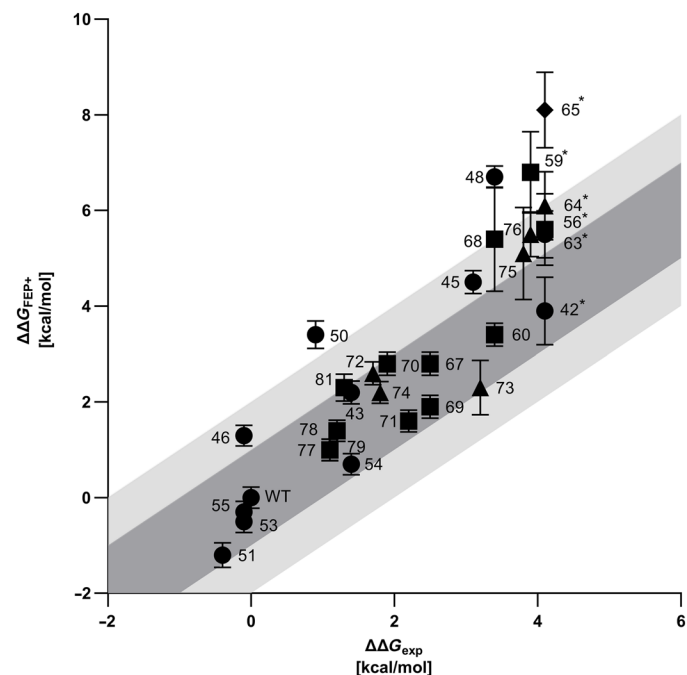


**Fig. 4. FEP values can predict mutational effects on LEN binding affinity.** Mean experimental fold change values ( $\Delta\Delta G_{exp}$ ) are plotted versus predicted fold change values ( $\Delta\Delta G_{FEP}$ ) with predicted cycle closure error as error bars. Gibbs free energy values are reported in kcal/mol. Shaded regions represent  $\pm 1$  and  $\pm 2$  kcal/mol deviation. The WT and single mutants are highlighted as circles (42: M66I; 43: Q67H; 44: Q67K; 45: K70H; 46: K70R; 47: K70S; 48: K70N; 50: N74D; 51: N74K; 53: A105T; 54: T107N; 55: T107S), double mutants as squares (56: M66I+Q67H; 57: M66I+K70S; 59: M66I+N74D; 60: M66I+A105T; 61: M66I+T107S; 66: Q67K+K70H; 67: Q67H+K70R; 68: Q67H+N74D; 69: Q67H+A105T; 70: Q67H+T107N; 71: Q67H+T107S; 76: K70N+N74K; 77: K70R+A105T; 78: K70R+T107N; 79: K70R+T107S; 81: N74D+A105T), triple mutants as triangles (62: M66I+Q67H+K70R; 63: M66I+Q67H+A105T; 64: M66I+N74D+A105T; 72: Q67H+K70R+A105T; 73: Q67H+K70R+T107N; 74: Q67H+K70R+T107S; 75: Q67H+N74D+A105T), and the quadruple mutant (65: M66I+Q67H+N74D+A105T) is displayed as a diamond. Asterisk indicates experimental data beyond assay limit of quantification (fold change value > 1000, which equates to >4.1 kcal/mol).

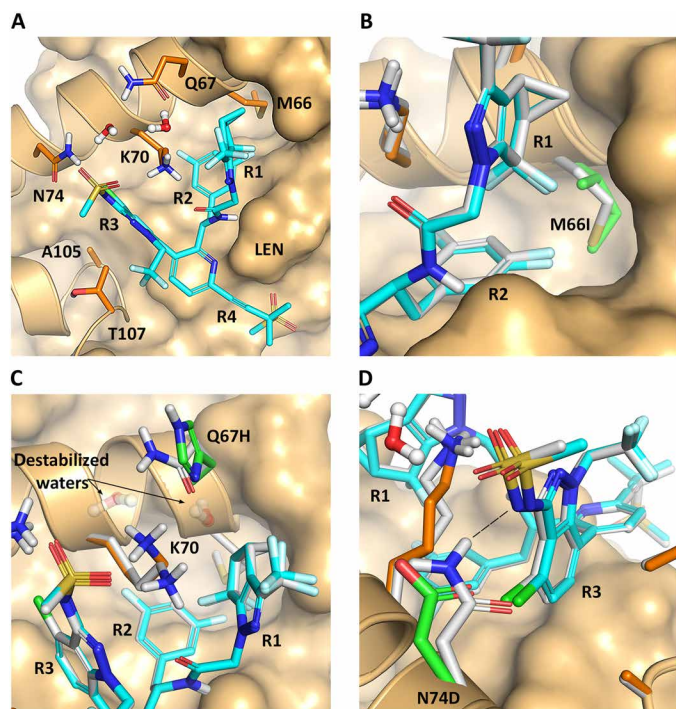


**Fig. 5. LEN resistance-associated mutations disrupt key hydrophobic and hydrogen bond interactions, reducing binding affinity and potency.** (A) LEN [shown in cyan; PDB: 6V2F (7)] binds at the interface between two capsid protein subunits. Residues discussed in this work (M66, Q67, K70, N74, A105, and T107) are shown in detail. (B) Overlay of the predicted structure for M66I with the WT structure. The mutated residue is shown in green, with other residues from the M66I prediction shown in orange. The reference WT residues (including bound LEN) are each shown in white. (C) Overlay of the predicted structure for Q67H with the WT structure, using a similar color scheme as above. The destabilized water molecules are displayed as faint red and white balls and sticks. (D) Overlay of the predicted structure for N74D in green with the WT structure in white, using a similar color scheme.

R1 and R2 groups. K70 formed a cation- $\pi$  interaction with R1/R3 and contributed to a hydrogen bond network involving Q67, two ordered water molecules, the R3 sulfonamide, and the R1/R2 amide linker. N183 from CA-2 also supported this network. N74 added a hydrogen bond to the deprotonated R3 sulfonamide, and A105 and T107 provided a hydrophobic surface.

With respect to the large shift in LEN potency associated with the M66I mutation, we observed that this residue is in direct contact with two hydrophobic groups on LEN: the fused tricyclic [3.1.0]-pyrazole R1 group and the 3,5-difluorobenzyl R2 group. The M66I substitution (Fig. 5B and table S4) resulted in the greatest resistance among capsid single mutations, with a predicted decrease in binding affinity of  $\Delta\Delta G = 3.9$  kcal/mol. This seemed to stem from reshaping of the hydrophobic pocket. Specifically, the introduction of branching at the amino acid  $\beta$  carbon added bulk and rigidity, forcing the LEN R1 and R2 groups to fit in a tighter space.

Substitutions at capsid protein residues Q67 or K70 were predicted to disrupt the hydrogen bond network critical for LEN binding. For the Q67H mutation (Fig. 5C), the hydrogen bond to the R3 bridging water was lost. This loss also disrupted the second water

molecule, destabilizing K70. The disruption of this hydrogen bond network was consistent with the observed 10.2-fold reduction in LEN potency (predicted change in binding affinity of  $\Delta\Delta G = 2.2$  kcal/mol). A similar situation was observed for substitutions of either Q67H/K or K70H/N/R (fig. S5). For N74D (Fig. 5D), the substitution of asparagine with negatively charged aspartic acid introduced a repulsion with the negatively charged R3 sulfonamide. This repulsion may have been mitigated by a conformational change, but at minimum, a favorable hydrogen bond was lost. Last, A105 and T107 were located on a loop of helix 6 with flexibility. The substitutions A105T and T107N/S had minimal impact on LEN binding (fig. S6 and table S3).

Further examination of the hydrogen bond network in the LEN binding pocket (Fig. 6A), including mutations at positions Q67 and K70, suggested that double mutations may cause greater destabilization. The Q67H substitution resulted in loss of the hydrogen bond to the R3 bridging water (Fig. 6B). The K70R mutation displaced one of two associated water molecules but compensated by forming new hydrogen bonds and a cation- $\pi$  stacking interaction with the R1 and R3 groups, consistent with LEN's retained potency (Fig. 6C). In addition, we observed that Q67 stabilized the arginine in K70R, a

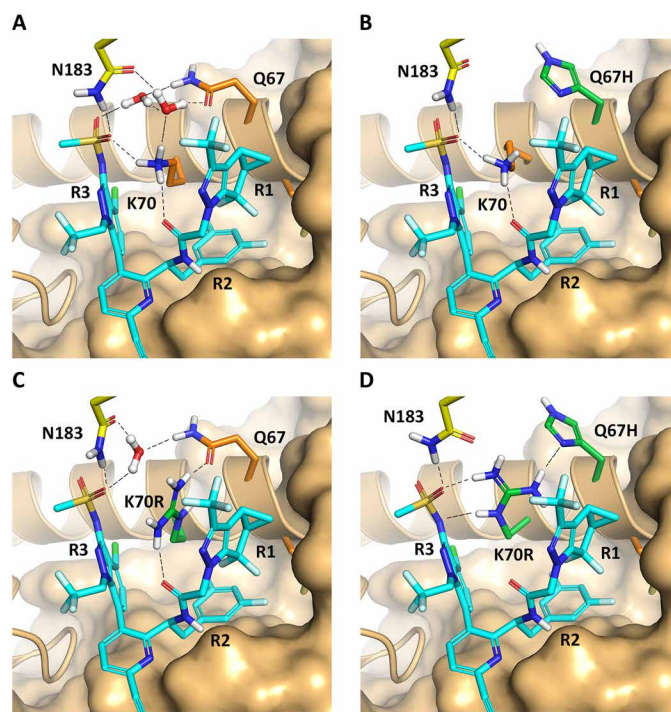


**Fig. 6. Double mutation Q67H+K70R further destabilizes the LEN binding pocket by disrupting hydrogen bond networks, compromising LEN potency.** (A) In the WT binding site, LEN (shown in cyan) forms an extensive hydrogen bond network (black dashed lines) between the capsid residues Q67, K70, and N183; two water molecules (shown as red and white sticks and balls); the R1/R2 amide linker; and the R3 sulfonamide of LEN. (B) The Q67H single mutation is highlighted in green, and LEN is presented in cyan. The black dashed lines indicate hydrogen bonds. (C) The K70R mutation is presented in green, and Q67 is highlighted in orange. LEN is displayed in cyan. Water molecules are shown as red and white sticks and balls. The hydrogen bond network is illustrated as black dashed lines. (D) The Q67H+K70R double mutant is shown in green. The hydrogen bond network is presented as black dashed lines.

role lost in the Q67H+K70R mutants, thereby compromising LEN interactions (Fig. 6D).

## DISCUSSION

The emergence of resistance to antiretroviral therapies poses challenges in managing HIV-1 infection and has been an important driver for the development of additional therapeutic options. As the first-in-class capsid inhibitor, LEN offers a therapeutic option for HIV-1 treatment and PrEP. Our study examined the molecular interactions between LEN and clinically observed capsid variants to address mechanisms of LEN resistance and their impact on HIV-1 fitness. The insights from this study may help guide the design of next-generation capsid inhibitors with improved resistance profiles and inform strategies for their clinical use, particularly in treatment-experienced populations (17).

In the phase 2/3 CAPELLA study, a subset of heavily treatment-experienced PLWH developed capsid RAMs while receiving LEN functional monotherapy, either because of nonadherence to their optimized background regimen or the absence of fully active agents in the optimized background regimen owing to preexisting resistance (14). LEN's long-acting nature presents a unique feature: Once administered, it stays in circulation for months, making rapid removal from a failing regimen unpractical. Therefore, maintaining LEN in combination with an active optimized background regimen is critical to suppress viral replication and minimize the risk of resistance emergence. Viral suppression remains achievable when LEN is paired with active agents (14), reinforcing the need for careful regimen design and close monitoring. In this context of LEN functional monotherapy, the high viral selective pressure combined with the long-acting pharmacokinetics of LEN led to the emergence of the capsid RAMs that we characterized here.

Clinical observations from CAPELLA illustrate the nuanced relationship between replication capacity and clinical outcome under LEN selective pressure. Participant 1 initially experienced virologic failure with M66I alone (resulting in a replication capacity of 17%, Table 2; fig. S3), achieved resuppression to <50 copies/ml, but later rebounded above baseline (14) after acquiring N74D and A105T mutants, increasing replication capacity to 34%. Similarly, Participant 10 had a baseline replication capacity of 112.9% and HIV-1 RNA of 85,100 copies/ml, acquired M66I+N74D+A105T (resulting in a replication capacity of 46.6%), and later rebounded to 7510 copies/ml with M66I+Q67H+N74D+A105T (a replication capacity of 64.2%). Additional CAPELLA cases with complex LEN RAMs (e.g., M66I+Q67H+K70R or M66I+T107A) confirmed that viruses with replication capacity values well below 100% can sustain high-level viremia. These findings underscore that *in vitro* replication capacity reflects relative viral fitness but is not a reliable predictor of clinical suppression given that compensatory mutations can restore replication enough to permit rebound. This trajectory mirrors patterns observed with PI- and INSTI-resistance pathways, supporting the translational relevance of replication capacity as a qualitative, but not quantitative, indicator of viral fitness under selective drug pressure.

Capsid RAMs were associated with varying degrees of LEN resistance that, in turn, inversely correlated with reductions in replication capacity. These findings reflect the long-held paradigm that WT HIV-1 is the most fit species in an individual and that resistance mutation acquisition typically reduces viral fitness

(18). The relationship between resistance and replication capacity impairment has also been well documented for other antiretroviral classes. Resistance to PIs is often characterized by a gradual accumulation of mutations in the protease, corresponding to increasing magnitude of phenotypic resistance (18–21). Early PI-resistant viruses frequently exhibited reduced replication capacity (18, 21–24), which was partially or fully restored upon emergence of compensatory mutations, such as L63P or M46I, that exist as polymorphisms in the protease sequence (22, 23) or mutations near protease cleavage sites, such as L449F or P453L in *gag* (24). In contrast with the gradual resistance acquisition seen with PIs, we found that LEN resistance can arise from a single highly resistant mutation, M66I, which substantially reduced LEN binding affinity to CA-M66I hexamers (1, 25). Earlier studies investigating SDMs reported a strong reduction in replication capacity for M66I [ $<1\%$ ; (26)]. However, the clinical sample in our study with M66I alone resulted in a replication capacity of 17.1%. This discrepancy may reflect the contribution of natural genetic variation to viral fitness, which is absent in the context of XXLAI SDMs, as previously noted for PI and RT mutants (27). Unlike M66I, the Q67H resistance pathway led to minor resistance to LEN (median of 4.7-fold across assays) and maintained near-WT replication capacity in most samples. This was consistent between SDMs [5.7-fold reduced susceptibility to LEN and 100% replication capacity; (26)] and clinical isolates. Higher LEN phenotypic resistance was observed upon Q67H+K70R emergence, which was generally associated with near-WT replication capacity. However, replication capacity reductions were still apparent in samples with these mutations, suggesting that sequence context may influence the fitness impact of the Q67H/K70R pathway.

Similarly to PIs, INSTI resistance also showed a fitness-resistance trade-off comparable to our findings for LEN. For raltegravir and elvitegravir, primary mutations such as Q148R or N155H reduced replication capacity to 36 to 72% of WT, whereas dual mutations (e.g., Q148R+N155H) decreased replication capacity to 4 to 20% (28, 29). Dolutegravir-resistance pathways involving G118R and R263K showed marked impairment, with G118R alone reducing replication capacity to 34% and the G118R+R263K combination to below 10% of WT (30, 31). Additional studies confirmed that early INSTI-resistant viruses often exhibited severe fitness losses, which were partially mitigated by secondary mutations (32, 33). However, in our study, single INSTI RAMs such as N155H and R263K retained high replication capacity (82 and 85%, respectively). In contrast, most Q67H±K70R variants maintained near-baseline replication, highlighting the heterogeneity in fitness costs among LEN RAMs. These observations underscore the role of compensatory mutations in restoring fitness while increasing resistance (29, 31–33). RAMs targeting NRTIs and NNRTIs are commonly associated with impaired replication capacity, although the extent of fitness loss varies by mutation and sequence context.

LEN-resistance mutations, such as M66I and K70N, can negatively affect various aspects of HIV-1 replication, including capsid protein assembly, capsid intracellular trafficking, nuclear pore binding, and integration, leading to impaired HIV-1 replication (25, 34, 35). The more pronounced effect of LEN RAMs in decreasing viral replication compared with other antiretrovirals may be attributed to the critical role of maintaining optimal capsid integrity to achieve essential steps in the viral replication cycle (25, 36, 37). Another potential consequence of the reduced fitness associated with capsid RAMs is the loss of binding to host cell nuclear import

factors (25). Cleavage and polyadenylation specificity factor 6 (CPSF6) plays a crucial role in the nuclear import of HIV-1 reverse transcription complexes (38). Data suggest that LEN might block the viral cDNA nuclear import by competing with host-cell nuclear import factors, like CPSF6 (1). The N74D substitution in capsid protein disrupts CPSF6 binding and alters the nuclear entry route, resulting in an abnormal viral accumulation at the nuclear periphery and integration in transcriptionally inactive parts of the host genome (38, 39). Our findings reinforced that acquiring LEN RAMs in capsid can drastically impair overall viral fitness, including diminished particle infectivity and replication capacity (Table 2, figs. S3 and S4, and table S2).

The MT-2 assay, which relies on virus-induced cell killing, has limited sensitivity for HIV-1 variants with replication defects. Several CA-mutated strains (e.g., M66I) showed insufficient cytopathic effects in MT-2 cells, creating gaps in characterizing the full viral diversity. Capsid mutations appeared to impair infectivity more profoundly than previously observed for PR, RT, and IN mutants (40, 41). Although RT mutations like M184V/I resulted in replication capacity deficiency, their infectivity remained higher than that for most capsid mutants (41), suggesting that capsid mutations may exert a stronger impact on viral replication. The RevLun reporter assay provided greater sensitivity for detecting replication-deficient capsid mutants. These cells encode a Rev-dependent reporter system that relies on HIV infection rather than requiring viral killing of the cells (42). Our findings validate the use of RevLun assay for phenotypic resistance testing, particularly for viruses with replication defects (43).

We found that the capsid mutations M66I, N74D, Q67H/K, K70R/H/N, Q67H+K70R, and Q67K+K70H altered capsid protein tertiary structure and function. The M66I mutation, located in helix 4, was previously shown to disrupt capsid protein assembly, stability, and nuclear import (25). We found that the M66I mutation reshaped the hydrophobic pocket, reduced flexibility, and introduced steric hinderance to LEN binding. Mutations Q67H/K and K70R/H/N have been shown to negatively affect capsid integrity (1, 8, 34). We observed that changes in Q67 or K70 disrupted the hydrogen bond network critical for LEN binding, where Q67 bridges a water molecule between capsid protein and LEN. This destabilization was associated with increased LEN. Mutation pairs Q67H+K70R and Q67K+K70H further altered capsid protein architecture, which was associated with compromised LEN binding and enhanced LEN resistance. The N74D mutation introduced electrostatic repulsion with the negatively charged sulfonamide, altering the binding pocket. Situated near the cyclophilin A binding loop (helices 4 and 5), N74D may affect host protein interactions (e.g., CPSF6), affecting capsid trafficking and nuclear import (44, 45). These mutations highlight the structural sensitivity of capsid protein and its impact on HIV-1 replication. These insights may inform the design of next-generation inhibitors targeting resistant strains.

One limitation of this study is that we only queried sequence variants in *gag* and did not include other genomic regions (e.g., envelope) that can influence antiretroviral resistance (46). In addition, the RAMs inserted into the *gag* region of XXLAI did not include polymorphisms that were present in the clinical isolates, precluding the study of compensatory effects of these polymorphic residues on capsid resistance. We observed substantial variability in LEN EC<sub>50</sub> fold change values among isolates harboring the same primary mutation (e.g., M66I or Q67H+K70R), suggesting that additional

polymorphisms, either in *gag* or other regions in the HIV-1 genome, may modulate LEN susceptibility. Our dataset was underpowered to identify consistent secondary or compensatory mutations because of the limited sample size. Another limitation is that structural interpretations of LEN binding were based on the WT capsid protein cocrystallized with LEN (1). Individual capsid mutants (single and double mutants) were not analyzed by x-ray crystallography, which limits direct structural insights into how these mutations alter LEN binding. Future studies including full-genome sequencing may elucidate these additional contributors to resistance and viral fitness.

In conclusion, we have shown that the selective pressure exerted by LEN in situations of functional monotherapy has led to the emergence of capsid RAMs conferring various degrees of phenotypic resistance to LEN. In most cases, LEN resistance coincided with substantial replication capacity defects. Together, these data support the development of treatment regimens that combine LEN with other active antiretrovirals to maintain durable suppression.

## MATERIALS AND METHODS

### Study design

The objective of this study was to investigate the impact of clinically observed capsid RAMs on LEN susceptibility and viral replication and to identify how these mutations affected structural interactions between LEN and the capsid protein. We combined phenotypic assays, structural modeling, and mutational analyses to characterize the functional consequences of individual and combinatorial capsid RAMs. The study design was informed by resistance profiles emerging from clinical trials and aimed to elucidate the biological mechanisms underlying LEN resistance and its fitness costs. Each data point derived from either the MT-2 assay or the RevLun assay represents at least three biological replicates, each with three technical replicates. For viral outgrowth assays in PBMCs, data are shown as means  $\pm$  SD from at least three biological replicates, each with four technical replicates. Patient informed consent was obtained before collection and use of the clinical samples used in this study. These plasma samples were from participants who were naive to the capsid inhibitor class before enrollment into the studies.

### Amino acid representation

Throughout this manuscript, amino acid sequences are presented using the single-letter code rather than the three-letter code for clarity and brevity. The single-letter abbreviations for the 20 standard amino acids are as follows: A (Ala) for alanine, C (Cys) for cysteine, D (Asp) for aspartic acid, E (Glu) for glutamic acid, F (Phe) for phenylalanine, G (Gly) for glycine, H (His) for histidine, I (Ile) for isoleucine, K (Lys) for lysine, L (Leu) for leucine, M (Met) for methionine, N (Asn) for asparagine, P (Pro) for proline, Q (Gln) for glutamine, R (Arg) for arginine, S (Ser) for serine, T (Thr) for threonine, V (Val) for valine, W (Trp) for tryptophan, and Y (Tyr) for tyrosine. This notation follows the recommendations of the International Union of Pure and Applied Chemistry (IUPAC) for amino acid abbreviations and is used to facilitate concise reporting of mutations and sequence alignments.

### Compounds and cell culture reagents

LEN and control compounds were synthesized at Gilead Sciences Inc. GlutaMAX RPMI 1640, Gibco Dulbecco's modified Eagle's medium (DMEM) high glucose, penicillin (10,000 U/ml), and streptomycin (10,000  $\mu$ g/ml) were purchased from Thermo Fisher Scientific. Fetal

bovine serum (FBS) was obtained from HyClone Laboratories. Media were supplemented with 10% heat-inactivated FBS and with 5 ml each of penicillin (10,000 U/ml) and streptomycin (10,000 U/ml) per 500 ml of medium (complete DMEM or complete RPMI).

### Cell culture

The human embryonic kidney (HEK) cell line HEK293T was purchased from the American Type Culture Collection and maintained at <80% confluency in complete DMEM. The human lymphoblastoid cell line MT-2 was obtained from the AIDS reagent repository. The Rev-dependent HIV-1 reporter T cell line Rev-CEM-Luc/GFP (referred herein as RevLun) (42) was purchased from Virongy Biosciences Inc. Both T cell lines were maintained in complete RPMI 1640. Human PBMCs purchased from AllCells were collected from healthy volunteers under informed consent; their use was approved by AllCells. Human PBMC cultures were prepared as previously described (47). Before infection, PBMCs were activated with phytohemagglutinin (PHA; 1 µg/ml; Sigma-Aldrich) and 10 IU/ml of recombinant human interleukin-2 (IL-2; Roche Diagnostics) for 48 hours at 37°C.

### Plasmids

The infectious molecular clone pXXLAI was kindly provided by J. Mellors. This plasmid was derived from the infectious clone pLAI3.2, which was modified to contain a *Xma*I and *Xba*I restriction site within the HIV *rt* gene to facilitate cloning (48). The plasmid pNL4-3-JRFL-secNLuc, encoding replication-competent HIV-1 and secreted NanoLuc luciferase (secNLuc), was previously described (9).

### HIV-1 and recombinant HIV-1

HIV-1 isolates containing the Gag-PR encoding DNA fragment were generated from baseline and postbaseline treatment-naïve and heavily treatment-experienced patient-derived plasma samples from the clinical studies CALIBRATE and CAPELLA. Plasma samples (140 µl) were treated with 1 µl of DNase I (catalog no. 04716728001, Roche) and 2 µl of 1 M MgCl<sub>2</sub> for 45 min at room temperature. Viral RNA was extracted using the QIAamp Viral RNA mini kit (Qiagen) and eluted in 60 µl. Viral RNA was reverse-transcribed into cDNA using Ready-To-Go You-Prime first-strand beads (GE Healthcare) using random hexamers (catalog no. N8080127, Thermo Fisher Scientific) at a final concentration of 1.5 mM. The HIV-1 gag-pro DNA fragments were amplified by two rounds of polymerase chain reaction [PCR; Platinum Super Fi II PCR Master Mix (#12368010), Thermo Fisher Scientific] using the first- and second-round primers described in table S5 (49). For the multicycle replication kinetics assay in human PBMCs, the CA-encoding regions containing RAMs were amplified using the respective pXXLAI construct as a template and inserted into pNL4-3-JRFL-secNLuc via *Bss*HIII-*Xma*I ligation (9).

SDMs within the CA-encoding region of the pXXLAI *gag* gene were generated by overlap extension PCR (50, 51). The generation of overlapping regions of two PCR fragments allowed their annealing in a subsequent PCR, which contained the respective SDM resulting in the amino acid substitution of interest (table S2). A total of 44 SDMs were generated, containing single, double, triple, or quadruple mutations at positions previously observed in participants with emergent LEN RAMs in capsid in the studies CAPELLA and CALIBRATE.

Replication-competent pXXLAI encoding either treatment-emergent capsid RAMs or capsid SDMs were transfected into

HEK293T cells using Lipofectamine 3000 transfection reagent (Invitrogen) with 7 µg of proviral plasmid in 2 million HEK293T cells seeded in T-25 cell culture flasks with 6 ml of complete DMEM media 1 day before transfection. Cell-free virus-containing cell culture supernatants were harvested after 48 and 72 hours, stored at –80°C, and tested for infectivity in titration assays.

Replication-competent HIV-1 encoding the secreted NanoLuc reporter was generated by transfecting HEK293T cells with pNL4.3-JRFL-secNLuc plasmids using Lipofectamine 3000. Twenty-four micrograms of the pNL4-3 plasmid was transfected in 4.75 million HEK293T cells seeded in T-75 flasks with 15 ml of complete DMEM. The cell-free viral supernatant was collected 2 days posttransfection and concentrated using the Lenti-X Concentrator (Clontech Laboratories Inc.) for at least 24 hours at 4°C. Viruses were pelleted at 1500g for 1 hour, resuspended in a 10× lower volume of complete RPMI, and stored at –80°C as single-use aliquots. HIV quantities in each sample were assessed by luciferase assay as described below (Nano-Glo Luciferase Assay reagent).

### HIV-1 infectivity titration assay

Viral infectivity of subcloned clinical samples and SDMs was tested in a titration assay using luciferase-based viability (MT-2 assay) or infectivity readout (RevLun assay) to determine the optimal viral supernatant input volume for use in phenotypic assays. Briefly, 2.4 million cells of the respective cell type were added to 1000 µl of the viral supernatant and incubated at 37°C with gentle rocking for 2.5 hours. Infected cells were diluted to a concentration of 0.17 million cells/ml (1:14 dilution) in complete RPMI media. The cells were further serially diluted (1:3) with uninfected cells at the same concentration to study the infectivity of decreasing viral inputs. Nine viral dilutions were tested per construct and plated in triplicate (3 × 50 µl) into a 96-well plate (black plates with clear bottom, Corning) in the presence (fully protected to HIV-1 infection) or absence (fully susceptible to HIV-1 infection) of 300 nM dolutegravir. After 5 days of incubation at 37°C, 5% CO<sub>2</sub>, and 95% humidity, 100 µl of CellTiter-Glo (MT-2 assay) or ONE-Glo reagent (RevLun assay) was added to each well and the luminescence signal was quantified using an Envision plate reader (PerkinElmer). The ratio between the dolutegravir-protected wells (maximum cell survival or minimum infectivity) and the unprotected wells (minimum cell survival and maximum infectivity) was used to determine viral infectivity.

### HIV-1 antiviral phenotypic MT-2 and RevLun assays

Susceptibility of clinical samples and capsid SDM viruses to LEN and control compounds was determined in MT-2 or RevLun 5-day multicycle antiviral assays (26, 43). Briefly, 2.4 million cells were incubated with virus for 2.5 hours at 37°C in a 1.2-ml screw cap tube using a viral input yielding a signal-to-noise ratio in the range of 4 to 7 for the MT-2 assay and greater than 4 for the RevLun assay, according to the infectivity results obtained in the virus titration assay. Serial dilutions (1:5) of LEN were prepared, and 50 µl was transferred into a 96-well plate (black, clear-bottom 96-well plate, Corning) in triplicate. After incubation, the cells were diluted 1:14 (0.17 cells/ml) in media. Fifty microliters of HIV-infected cell suspensions was transferred to all wells. After 5 days of incubation at 37°C (5% CO<sub>2</sub>, 95% humidity), 100 µl of CellTiter-Glo (Promega) for MT-2 assay or 100 µl of OneGlo (Promega) for RevLun assay was added to each well, and luminescence was measured using an Envision plate reader. The percentage inhibition of cell viability in the

drug-containing wells relative to fully protected dolutegravir control was used to generate antiviral dose-response curves and calculate EC<sub>50</sub> values using XLfit (IDBS). The limit of quantification was a fold change of >1000 compared to WT virus.

### Monogram Gag-Pro HIV-1 antiviral phenotypic assay

Resistance test vectors were generated at Monogram Biosciences. Briefly, sequences encompassing the entire Gag and PR coding regions were ligated into an HIV-1 NL4-3 derived test vector containing a luciferase gene and lacking the *env* gene. Pseudotyped virus stocks were generated by cotransfection of test vectors with an amphotropic murine leukemia virus *env* containing vector in HEK293T cells as previously described (52). Phenotypic susceptibilities of the pseudotyped virus stocks to LEN and control drugs were assessed at Monogram Biosciences using the PhenoSense Gag-Pro single-cycle assay (52). Pseudotyped virus stocks were generated in HEK293T cells in the presence of serially diluted drugs (LEN and comparator compounds) and were used to infect fresh HEK293T cells in the antiviral assay. Luciferase gene expression was quantified after 2 days. Drug susceptibility data were analyzed by plotting the percentage inhibition of luciferase activity versus log<sub>10</sub> drug concentration. Inhibition curves defined by the four-parameter sigmoidal function  $f(x) = a - [b/1 + (x/c)^d]$ , where  $a$  is the upper asymptote,  $b$  is the range (difference between upper and lower asymptotes),  $c$  is the inflection point (EC<sub>50</sub> or midpoint), and  $d$  is the slope (Hill coefficient), were fit by nonlinear least-squares and bootstrapping to calculate EC<sub>50</sub> values. Fold change in drug susceptibility was determined by dividing the EC<sub>50</sub> of the clinical or SDM isolate-derived virus by that of a reference virus containing the WT NL4-3 HIV-1 sequence. The limit of quantification was a fold change of 2700 compared with WT virus. Replication capacity was presented as the percentage of luciferase activity in pseudotyped virus-infected cells relative to the reference strain (NL4-3).

### Resistance categorization

Phenotypic susceptibility to LEN was assessed using the MT-2, RevLun, and PhenoSense Gag-Pro assays described above. Viral clones containing participant-derived or SDMs in the capsid region of *gag* were generated and tested for LEN susceptibility. The EC<sub>50</sub> values were determined for each variant and compared to the WT reference strain (XXLAI) to calculate the fold change in drug susceptibility. Resistance categories were defined on the basis of fold change values as follows: 0 to 3.5, no resistance; >3.5 to 25, low resistance; >25 to <100, medium resistance; >100, high resistance. All assays were performed in triplicate, and data were analyzed using XLfit.

### Virus outgrowth kinetics in human PBMCs

Human PBMCs from two independent donors were purchased from AllCells and activated in complete RPMI supplemented with recombinant human IL-2 (10 IU/ml) and PHA (1 µg/ml) in a humidified 37°C incubator for 48 hours. On day 0,  $6 \times 10^6$  activated PBMCs were resuspended in complete RPMI supplemented with IL-2 (10 IU/ml) and DEAE-dextran (10 µg/ml) (Sigma-Aldrich) and were infected in bulk culture with equal volumes of NL4-3-JRFL-secNLuc reporter HIV-1 viruses encoding the *gag* fragment from each clinical isolate for 3 hours at 37°C. NL4-3-JRFL-secNLuc reporter viruses were produced in parallel. Infected cell suspensions were pelleted and adjusted to  $1 \times 10^6$  cells/ml. HIV-infected PBMCs ( $2 \times 10^5$ )

were added to four replicate wells per time point. Assay plates were incubated for 14 days at 37°C in a humidified incubator. At indicated time points, 2 µl of the cell-free supernatant was collected from each well and luminescence was measured following Nano-Glo addition as described above.

### Structural analyses

The cross-linked hexameric cocrystal structure of HIV-1 capsid protein in complex with LEN [Protein Data Bank (PDB): 6V2F] (1) was truncated to two adjacent capsid protein monomers and prepared for modeling using Schrödinger's Protein Preparation procedure [PyMOL Molecular Graphics System Version 3.1 Schrödinger LLC; (53, 54)]. This procedure adds protons, optimizes the hydrogen bonding network, and carries out a restrained optimization. Protein FEP selectivity calculations were conducted to estimate changes in LEN binding-free energy relative to capsid mutations. Simulations were conducted with Schrödinger's Protein FEP<sup>+</sup> using the standard simulation, sampling, and force-field parameters (55) and extended to 10 ns to improve convergence. Fold change values were converted to Gibbs free energies by using  $\Delta G^\circ = -R \cdot T \cdot \ln(K_{eq})$ , where  $\Delta G^\circ$  is the standard Gibbs free energy (in joules per mole, J/mol),  $R$  is the universal gas constant [8.314 J/(mol K)],  $T$  is the absolute temperature in Kelvin (K), and  $\ln(K_{eq})$  is the natural logarithm of the equilibrium constant, calculated at 25°C, assuming equilibrium, constant pressure, and constant temperature. Kendall's Tau (56), implemented in SciPy 1.15.2, was used to determine rank-ordering power of FEP<sup>+</sup> across 24 variants with nonqualified experimental data. Predicted FEP errors were calculated using the cycle closure method (57), as implemented in Schrödinger's Protein FEP<sup>+</sup>.

Additional structural analyses of mutation-induced changes were performed using sidechain conformational search in Schrödinger's MacroModel (54). Residues in direct contact with mutated sites were included in Monte Carlo Multiple Minimum sampling, whereas LEN and all residues within 7 Å of LEN were allowed to relax. Sampling was done for 300 steps. Resulting structures were tested for stability using a 20-ns molecular dynamics simulation in Schrödinger's Desmond.

### Statistical analysis

Data from MT-2 and RevLun antiviral assays are shown as mean (fig. S2 and table S1) or median with IQR and min-max whiskers (Fig. 1 and Table 1). Each data point represents at least three biological replicates, each with three technical replicates. Correlation analyses were performed using simple linear regression;  $r^2$  values are reported (Fig. 2). For viral outgrowth assays in PBMCs, data are shown as means ± SD from at least three biological replicates, each with four technical replicates (Table 2 and figs. S3 and S4). LEN susceptibilities to SDM capsid mutants are shown as mean experimental fold change versus predicted fold change with cycle closure error bars (Fig. 4).

### Supplementary Materials

#### The PDF file includes:

Figs. S1 to S6  
Tables S1 to S5

Other Supplementary Material for this manuscript includes the following:  
MDAR Reproducibility Checklist

## REFERENCES AND NOTES

- J. O. Link, M. S. Rhee, W. C. Tse, J. Zheng, J. R. Somoza, W. Rowe, R. Begley, A. Chiu, A. Mulato, D. Hansen, E. Singer, L. K. Tsai, R. A. Bam, C. H. Chou, E. Canales, G. Brizgys, J. R. Zhang, J. Li, M. Graupe, P. Morganello, Q. Liu, Q. Wu, R. L. Halcomb, R. D. Saito, S. D. Schroeder, S. E. Lazerwith, S. Bondy, D. Jin, M. Hung, N. Novikov, X. Liu, A. G. Villaseñor, C. E. Cannizzaro, E. Y. Hu, R. L. Anderson, T. C. Appleby, B. Lu, J. Mwangi, A. Liclican, A. Niedziela-Majka, G. A. Papalia, M. H. Wong, S. A. Leavitt, Y. Xu, D. Koditek, G. J. Stepan, H. Yu, N. Pagratis, S. Clancy, S. Ahmadyar, T. Z. Cai, S. Sellers, S. A. Wolckenhauer, J. Ling, C. Callebaut, N. Margot, R. R. Ram, Y. P. Liu, R. Hyland, G. I. Sinclair, P. J. Ruane, G. E. Crofoot, C. K. McDonald, D. M. Brainard, L. Lad, S. Swaminathan, W. I. Sundquist, R. Sakowicz, A. E. Chester, W. E. Lee, E. S. Daar, S. R. Yant, T. Cihlar, Clinical targeting of HIV capsid protein with a long-acting small molecule. *Nature* **584**, 614–618 (2020).
- C. F. Kelley, M. Acevedo-Quinones, A. L. Agwu, A. Avihingsanon, P. Benson, J. Blumenthal, C. Brinson, C. Brites, P. Cahn, V. D. Cantos, J. Clark, M. Clement, C. Creticos, G. Crofoot, R. S. Diaz, S. Doblecki-Lewis, J. A. Gallardo-Cartagena, A. Gaur, B. Grinsztajn, S. Hassler, J. C. Hinojosa, T. Hodge, R. Kaplan, M. Lacerda, A. LaMarca, M. H. Losso, J. V. Madruga, K. H. Mayer, A. Mills, K. Mounzer, N. Ndlovu, R. M. Novak, A. P. Rios, N. Phanuphak, M. Ramgopal, P. J. Ruane, J. Sanchez, B. Santos, P. Schine, T. Schreibman, L. Y. Spencer, O. T. Van Gerwen, R. Vasconcelos, J. G. Vasquez, Z. Zwane, S. Cox, C. Deaton, R. Ebrahimi, P. Wong, R. Singh, L. B. Brown, C. C. Carter, M. Das, J. M. Baeten, O. Ogbuagu, PURPOSE 2 Study Team, Twice-yearly lenacapavir for HIV prevention in men and gender-diverse persons. *N. Engl. J. Med.* **392**, 1261–1276 (2024).
- L. G. Bekker, M. Das, Q. A. Karim, K. Ahmed, J. Batting, W. Brumskine, K. Gill, I. Harkoo, M. Jaggernath, G. Kigozi, N. Kiwanuka, P. Kotze, L. Lebina, C. E. Louw, M. Malahleha, M. Manentsu, L. E. Mansoor, D. Moodley, V. Naicker, L. Naidoo, M. Naidoo, G. Nair, N. Ndlovu, T. Palanee-Phillips, R. Panchia, S. Pillay, D. Potloane, P. Selepe, N. Singh, Y. Singh, E. Spooner, A. M. Ward, Z. Zwane, R. Ebrahimi, Y. Zhao, A. Kintu, C. Deaton, C. C. Carter, J. M. Baeten, F. M. Kiweewa, PURPOSE 1 Study Team, Twice-yearly lenacapavir or daily F/TAF for HIV prevention in cisgender women. *N. Engl. J. Med.* **391**, 1179–1192 (2024).
- Gilead Sciences Inc., SUNLENCA® (lenacapavir) tablets, for oral use. SUNLENCA® (lenacapavir) injection, for subcutaneous use. US Prescribing Information (2024); [https://www.gilead.com/-/media/files/pdfs/medicines/hiv/sunlenca/sunlenca\\_pi.pdf](https://www.gilead.com/-/media/files/pdfs/medicines/hiv/sunlenca/sunlenca_pi.pdf).
- O. Pornillos, B. K. Ganser-Pornillos, M. Yeager, Atomic-level modelling of the HIV capsid. *Nature* **469**, 424–427 (2011).
- E. M. Campbell, T. J. Hope, HIV-1 capsid: The multifaceted key player in HIV-1 infection. *Nat. Rev. Microbiol.* **13**, 471–483 (2015).
- M. Tsiang, A. Niedziela-Majka, M. Hung, D. Jin, E. Hu, S. Yant, D. Samuel, X. Liu, R. Sakowicz, A trimer of dimers is the basic building block for human immunodeficiency virus-1 capsid assembly. *Biochemistry* **51**, 4416–4428 (2012).
- S. M. Bester, G. Wei, H. Zhao, D. Adu-Ampratwum, N. Iqbal, V. V. Courouble, A. C. Francis, A. S. Annamalai, P. K. Singh, N. Shkriabai, P. Van Blerkom, J. Morrison, E. M. Poeschla, A. N. Engelman, G. B. Melikyan, P. R. Griffin, J. R. Fuchs, F. J. Asturias, M. Kvaratskhelia, Structural and mechanistic bases for a potent HIV-1 capsid inhibitor. *Science* **370**, 360–364 (2020).
- S. R. Yant, A. Mulato, D. Hansen, W. C. Tse, A. Niedziela-Majka, J. R. Zhang, G. J. Stepan, D. Jin, M. H. Wong, J. M. Ferreira, E. Singer, G. A. Papalia, E. Y. Hu, J. Zheng, B. Lu, S. D. Schroeder, K. Chou, S. Ahmadyar, A. Liclican, H. Yu, N. Novikov, E. Paoli, D. Goniak, R. R. Ram, M. Hung, W. M. McDougall, A. L. Brass, W. I. Sundquist, T. Cihlar, J. O. Link, A highly potent long-acting small-molecule HIV-1 capsid inhibitor with efficacy in a humanized mouse model. *Nat. Med.* **25**, 1377–1384 (2019).
- H. Dvory-Sobol, N. Shaik, C. Callebaut, M. S. Rhee, Lenacapavir: A first-in-class HIV-1 capsid inhibitor. *Curr. Opin. HIV AIDS* **17**, 15–21 (2022).
- R. Subramanian, J. Tang, J. Zheng, B. Lu, K. Wang, S. R. Yant, G. J. Stepan, A. Mulato, H. Yu, S. Schroeder, N. Shaik, R. Singh, S. Wolckenhauer, A. Chester, W. C. Tse, A. Chiu, M. Rhee, T. Cihlar, W. Rowe, B. J. Smith, Lenacapavir: A novel, potent, and selective first-in-class inhibitor of HIV-1 capsid function exhibits optimal pharmacokinetic properties for a long-acting injectable antiretroviral agent. *Mol. Pharm.* **20**, 6213–6225 (2023).
- N. A. Margot, V. Naik, L. VanderVeen, O. Anoshchenko, R. Singh, H. Dvory-Sobol, M. S. Rhee, C. Callebaut, Resistance analyses in highly treatment-experienced people with human immunodeficiency virus (HIV) treated with the novel capsid HIV inhibitor lenacapavir. *J. Infect. Dis.* **226**, 1985–1991 (2022).
- N. Margot, N. Pennetzdorfer, V. Naik, M. Rhee, C. Callebaut, Cross-resistance to entry inhibitors and lenacapavir resistance through week 52 in study CAPELLA. *Antivir. Ther.* **28**, 13596535231220754 (2023).
- N. A. Margot, V. Jogiraju, N. Pennetzdorfer, V. Naik, L. A. VanderVeen, J. Ling, R. Singh, H. Dvory-Sobol, O. Ogbuagu, S. Segal-Maurer, J. M. Molina, M. S. Rhee, C. Callebaut, Resistance analyses in heavily treatment-experienced people with HIV treated with the novel HIV capsid inhibitor lenacapavir after 2 years. *J. Infect. Dis.* **231**, 1239–1245 (2025).
- O. Ogbuagu, J. M. Molina, P. Chetchotisakd, M. N. Ramgopal, W. Sanchez, J. Brunetta, F. Castelli, G. E. Crofoot, C. C. Hung, S. Ronot-Bregigeon, N. A. Margot, H. Wang, H. Dvory-Sobol, M. S. Rhee, S. Segal-Maurer, Efficacy and safety of long-acting subcutaneous lenacapavir in heavily treatment-experienced people with multidrug-resistant HIV-1: Week 104 results of a phase 2/3 trial. *Clin. Infect. Dis.* **80**, 566–574 (2025).
- D. Hagins, M. Berhe, G. E. Crofoot, M. N. Ramgopal, J. Sims, C. McDonald, P. J. Ruane, W. E. Sanchez, A. Scribner, P. Benson, S.-Y. Liu, L. A. VanDerVeen, H. Dvory-Sobol, M. S. Rhee, S. K. Gupta, Final efficacy and safety of twice-yearly subcutaneous lenacapavir in treatment-naïve people with HIV: Randomized study. *AIDS* **2025**, 10.1097/QAD.0000000000004372 (2025).
- C. Wang, H. Huang, L. Valera, K. Parcella, C. Iwuagwu, B. McAuliffe, P. J. Falk, D. R. O'Boyle II, R. E. Rose, R. R. Padilla, C. Wu, Y. Xiong, J. Kadow, U. Hanumegowda, L. Sardo, E. P. Gillis, M. Krystal, R. A. Fridell, Preclinical virology profiles of the HIV-1 capsid inhibitors VH4004280 and VH4011499. *Antimicrob. Agents Chemother.* **69**, e0030925 (2025).
- M. Nijhuis, R. Schuurman, D. de Jong, J. Erickson, E. Gustchina, J. Albert, P. Schipper, S. Gulnik, C. A. B. Boucher, Increased fitness of drug resistant HIV-1 protease as a result of acquisition of compensatory mutations during suboptimal therapy. *AIDS* **13**, 2349–2359 (1999).
- J. H. Condra, W. A. Schleif, O. M. Blahy, L. J. Gabrylski, D. J. Graham, J. C. Quintero, A. Rhodes, H. L. Robbins, E. Roth, M. Shivaprakash, D. Titus, T. Yang, H. Teplert, K. E. Squires, P. J. Deutsch, E. A. Emini, In vivo emergence of HIV-1 variants resistant to multiple protease inhibitors. *Nature* **374**, 569–571 (1995).
- A. Carrillo, K. D. Stewart, H. L. Sham, D. W. Norbeck, W. E. Kohlbrener, J. M. Leonard, D. J. Kempf, A. Molla, In vitro selection and characterization of human immunodeficiency virus type 1 variants with increased resistance to ABT-378, a novel protease inhibitor. *J. Virol.* **72**, 7532–7541 (1998).
- J. G. Prado, T. Wrin, J. Beauchaine, L. Ruiz, C. J. Petropoulos, S. D. W. Frost, B. Clotet, R. T. D'Aquila, J. Martinez-Picado, Amprenavir-resistant HIV-1 exhibits lopinavir cross-resistance and reduced replication capacity. *AIDS* **16**, 1009–1017 (2002).
- M. Markowitz, M. Saag, W. G. Powderly, A. M. Hurley, A. Hsu, J. M. Valdes, D. Henry, F. Sattler, A. La Marca, J. M. Leonard, D. D. Ho, A preliminary study of ritonavir, an inhibitor of HIV-1 protease, to treat HIV-1 infection. *N. Engl. J. Med.* **333**, 1534–1540 (1995).
- J. Martinez-Picado, A. V. Savara, L. Sutton, R. T. D'Aquila, Replicative fitness of protease inhibitor-resistant mutants of human immunodeficiency virus type 1. *J. Virol.* **73**, 3744–3752 (1999).
- M. F. Maguire, R. Guinea, P. Griffin, S. Macmanus, R. C. Elston, J. Wolfram, N. Richards, M. H. Hanlon, D. J. T. Porter, T. Wrin, N. Parkin, M. Tisdale, E. Furfine, C. Petropoulos, B. W. Snowden, J.-P. Kleim, Changes in human immunodeficiency virus type 1 gag at positions L449 and P453 are linked to I50V protease mutants in vivo and cause reduction of sensitivity to amprenavir and improved viral fitness in vitro. *J. Virol.* **76**, 7398–7406 (2002).
- L. Briganti, A. S. Annamalai, S. M. Bester, G. Wei, J. R. Andino-Moncada, S. P. Singh, A. B. Kleinpetter, M. Tripathi, B. Nguyen, R. Radhakrishnan, P. K. Singh, J. Greenwood, L. I. Schope, R. Haney, S. W. Huang, E. O. Freed, A. N. Engelman, A. C. Francis, M. Kvaratskhelia, Structural and mechanistic bases for resistance of the M661 capsid variant to lenacapavir. *mBio* **16**, e0361324 (2025).
- N. Margot, L. Vanderveen, V. Naik, R. Ram, P. C. Parvangada, R. Martin, M. Rhee, C. Callebaut, Phenotypic resistance to lenacapavir and monotherapy efficacy in a proof-of-concept clinical study. *J. Antimicrob. Chemother.* **77**, 989–995 (2022).
- M. Pingen, A. M. J. Wensing, K. Fransen, A. De Bel, D. de Jong, A. I. M. Hoepelman, E. Magiorkinis, D. Paraskevis, M. M. Lunar, M. Poljak, M. Nijhuis, C. A. B. Boucher, SPREAD programme, Persistence of frequently transmitted drug-resistant HIV-1 variants can be explained by high viral replication capacity. *Retrovirology* **11**, 105 (2014).
- M. E. Abram, R. M. Hlhanich, D. D. Goodman, K. N. Andreatta, N. A. Margot, L. Ye, A. Niedziela-Majka, T. L. Barnes, N. Novikov, X. Chen, E. S. Svarovskaia, D. J. McColl, K. L. White, M. D. Miller, Impact of primary elvitegravir resistance-associated mutations in HIV-1 integrase on drug susceptibility and viral replication fitness. *Antimicrob. Agents Chemother.* **57**, 2654–2663 (2013).
- S. Fransen, M. Karmochkine, W. Huang, L. Weiss, C. J. Petropoulos, C. Charpentier, Longitudinal analysis of raltegravir susceptibility and integrase replication capacity of human immunodeficiency virus type 1 during virologic failure. *Antimicrob. Agents Chemother.* **53**, 4522–4524 (2009).
- M. A. Xiao, J. Cleyle, S. Yoo, M. Forrest, Z. Krullaars, H. T. Pham, T. Mesplède, The G118R plus R263K combination of integrase mutations associated with dolutegravir-based treatment failure reduces HIV-1 replicative capacity and integration. *Antimicrob. Agents Chemother.* **67**, e0138622 (2023).
- C. Vavro, T. Ruel, A. Wiznia, N. Montañez, K. Nangle, J. Horton, A. M. Buchanan, E. L. Stewart, P. Palumbo, Emergence of resistance in HIV-1 integrase with dolutegravir treatment in a pediatric population from the IMPAACT P1093 study. *Antimicrob. Agents Chemother.* **66**, e0164521 (2022).
- Z. Hu, D. R. Kuritzkes, Effect of raltegravir resistance mutations in HIV-1 integrase on viral fitness. *J. Acquir. Immune Defic. Syndr.* **55**, 148–155 (2010).
- M. Pollicita, M. Surodo, F. Di Santo, M. F. Cortese, L. Fabeni, V. Fedele, I. Malet, A. G. Marcelin, V. Calvez, F. Ceccherini-Silberstein, C. F. Perno, V. Svicher, Comparative replication capacity

- of raltegravir-resistant strains and antiviral activity of the new-generation integrase inhibitor dolutegravir in human primary macrophages and lymphocytes. *J. Antimicrob. Chemother.* **69**, 2412–2419 (2014).
34. S. M. Bester, D. Adu-Ampratwum, A. S. Annamalai, G. Wei, L. Briganti, B. C. Murphy, R. Haney, J. R. Fuchs, M. Kvaratskhelia, Structural and mechanistic bases of viral resistance to HIV-1 capsid inhibitor lenacapavir. *mBio* **13**, e0180422 (2022).
  35. S. J. Rihn, S. J. Wilson, N. J. Loman, M. Alim, S. E. Bakker, D. Bhella, R. J. Gifford, F. J. Rixon, P. D. Bieniasz, Extreme genetic fragility of the HIV-1 capsid. *PLOS Pathog.* **9**, e1003461 (2013).
  36. R. T. Schirra, N. F. B. Dos Santos, K. K. Zadrozny, I. Kucharska, B. K. Ganser-Pornillos, O. Pornillos, A molecular switch modulates assembly and host factor binding of the HIV-1 capsid. *Nat. Struct. Mol. Biol.* **30**, 383–390 (2023).
  37. J. C. V. Stacey, A. Tan, J. M. Lu, L. C. James, R. A. Dick, J. A. G. Briggs, Two structural switches in HIV-1 capsid regulate capsid curvature and host factor binding. *Proc. Natl. Acad. Sci. U.S.A.* **120**, e2220557120 (2023).
  38. A. N. Engelman, HIV capsid and integration targeting. *Viruses* **13**, 125 (2021).
  39. A. J. Price, A. J. Fletcher, T. Schaller, T. Elliott, K. Lee, V. N. KewalRamani, J. W. Chin, G. J. Towers, L. C. James, CPSF6 defines a conserved capsid interface that modulates HIV-1 replication. *PLOS Pathog.* **8**, e1002896 (2012).
  40. K. L. White, N. A. Margot, T. Wrin, C. J. Petropoulos, M. D. Miller, L. K. Naeger, Molecular mechanisms of resistance to human immunodeficiency virus type 1 with reverse transcriptase mutations K65R and K65R+M184V and their effects on enzyme function and viral replication capacity. *Antimicrob. Agents Chemother.* **46**, 3437–3446 (2002).
  41. M.-e. Cong, W. Heneine, J. G. Garcia-Lerma, The fitness cost of mutations associated with human immunodeficiency virus type 1 drug resistance is modulated by mutational interactions. *J. Virol.* **81**, 3037–3041 (2007).
  42. Y. Wu, M. H. Beddall, J. W. Marsh, Rev-dependent indicator T cell line. *Curr. HIV Res.* **5**, 394–402 (2007).
  43. S. Demirdjian, V. Naik, N. Margot, B. Falkard, C. Callebaut, Phenotypic characterization of replication-impaired lenacapavir-resistant HIV clinical isolates. *J. Med. Virol.* **97**, e70340 (2025).
  44. T. Schaller, K. E. Ocwieja, J. Rasaiyaah, A. J. Price, T. L. Brady, S. L. Roth, S. Hué, A. J. Fletcher, K. Lee, V. N. KewalRamani, M. Noursadeghi, R. G. Jenner, L. C. James, F. D. Bushman, G. J. Towers, HIV-1 capsid-cyclophilin interactions determine nuclear import pathway, integration targeting and replication efficiency. *PLOS Pathog.* **7**, e1002439 (2011).
  45. Z. Ambrose, K. Lee, J. Ndjomou, H. Xu, I. Oztop, J. Matous, T. Takemura, D. Unutmaz, A. Engelman, S. H. Hughes, V. N. KewalRamani, Human immunodeficiency virus type 1 capsid mutation N74D alters cyclophilin A dependence and impairs macrophage infection. *J. Virol.* **86**, 4708–4714 (2012).
  46. Y. Hikichi, R. Van Duynne, P. Pham, J. L. Groebner, A. Wiegand, J. W. Mellors, M. F. Kearney, E. O. Freed, Mechanistic analysis of the broad antiretroviral resistance conferred by HIV-1 envelope glycoprotein mutations. *mBio* **12**, e03134-20 (2021).
  47. M. Tsiang, G. S. Jones, J. Goldsmith, A. Mulato, D. Hansen, E. Kan, L. Tsai, R. A. Bam, G. Stepan, K. M. Stray, A. Niedziela-Majka, S. R. Yant, H. Yu, G. Kukulj, T. Cihlar, S. E. Lazerwith, K. L. White, H. Jin, Antiviral activity of bictegravir (GS-9883), a novel potent HIV-1 integrase strand transfer inhibitor with an improved resistance profile. *Antimicrob. Agents Chemother.* **60**, 7086–7097 (2016).
  48. C. Shi, J. W. Mellors, A recombinant retroviral system for rapid in vivo analysis of human immunodeficiency virus type 1 susceptibility to reverse transcriptase inhibitors. *Antimicrob. Agents Chemother.* **41**, 2781–2785 (1997).
  49. N. Margot, V. Naik, A. Nekkalapudi, A. Boopathy, B. Falkard, C. Callebaut, Rapid HIV-1 genotyping assay for the detection of capsid mutations. *J. Med. Virol.* **95**, e29292 (2023).
  50. R. M. Horton, H. D. Hunt, S. N. Ho, J. K. Pullen, L. R. Pease, Engineering hybrid genes without the use of restriction enzymes: Gene splicing by overlap extension. *Gene* **77**, 61–68 (1989).
  51. S. N. Ho, H. D. Hunt, R. M. Horton, J. K. Pullen, L. R. Pease, Site-directed mutagenesis by overlap extension using the polymerase chain reaction. *Gene* **77**, 51–59 (1989).
  52. C. J. Petropoulos, N. T. Parkin, K. L. Limoli, Y. S. Lie, T. Wrin, W. Huang, H. Tian, D. Smith, G. A. Winslow, D. J. Capon, J. M. Whitcomb, A novel phenotypic drug susceptibility assay for human immunodeficiency virus type 1. *Antimicrob. Agents Chemother.* **44**, 920–928 (2000).
  53. G. M. Sastry, M. Adzhigirey, T. Day, R. Annabhimoju, W. Sherman, Protein and ligand preparation: Parameters, protocols, and influence on virtual screening enrichments. *J. Comput. Aided Mol. Des.* **27**, 221–234 (2013).
  54. Schroedinger, Release notes (2024); <https://schrodinger.com/life-science/download/release-notes/>.
  55. L. Wang, Y. Wu, Y. Deng, B. Kim, L. Pierce, G. Krilov, D. Lupyán, S. Robinson, M. K. Dahlgren, J. Greenwood, D. L. Romero, C. Masse, J. L. Knight, T. Steinbrecher, T. Beuming, W. Damm, E. Harder, W. Sherman, M. Brewer, R. Wester, M. Murcko, L. Frye, R. Farid, T. Lin, D. L. Mobley, W. L. Jorgensen, B. J. Berne, R. A. Friesner, R. Abel, Accurate and reliable prediction of relative ligand binding potency in prospective drug discovery by way of a modern free-energy calculation protocol and force field. *J. Am. Chem. Soc.* **137**, 2695–2703 (2015).
  56. M. G. Kendall, The treatment of ties in ranking problems. *Biometrika* **33**, 239–251 (1945).
  57. L. Wang, Y. Deng, J. L. Knight, Y. Wu, B. Kim, W. Sherman, J. C. Shelley, T. Lin, R. Abel, Modeling local structural rearrangements using FEP/REST: Application to relative binding affinity predictions of CDK2 inhibitors. *J. Chem. Theory Comput.* **9**, 1282–1293 (2013).

**Acknowledgments:** We extend our thanks to the CALIBRATE and CAPELLA study participants, their families, and the participating study investigators and staff who made these studies possible. We thank S. Segal-Maurer (Gilead Sciences Inc.) and L. Selzer (Gilead Sciences Inc.) for thoughtful discussions and critical review of this manuscript. **Funding:** This work was supported and fully funded by Gilead Sciences Inc. **Author contributions:** N.P., N.A.M., and C.C. conceptualized the study and wrote the manuscript. N.P. and N.A.M. managed the study. N.P., V.N., and S.D. performed the drug susceptibility experiments. N.P., S.D., and M.R.H. performed the replication capacity experiments in PBMCs. C.S.J. and J.K.P. conducted the structural analyses, produced the structural images, and participated in writing the manuscript. S.R.Y., S.K.G., and O.O. provided draft text and critical review of the final text. All authors contributed to the review and editing of the manuscript. **Competing interests:** N.P., V.N., S.D., M.R.H., C.S.J., J.K.P., L.A.V., S.R.Y., H.D.-S., N.A.M., and C.C. are employees and stockholders of Gilead Sciences Inc., which funded the study. S.R.Y. is a coinventor on two granted patents covering the use of capsid inhibitors for HIV treatment (US11944611B2) and prevention (US11807625B2). O.O. has served as an advisor or consultant for Gilead Sciences Inc., ViiV Healthcare, and Janssen and has received honoraria from Gilead Sciences Inc. S.K.G. has received grant support from ViiV Healthcare and honoraria for participating on advisory boards for Gilead Sciences Inc. and ViiV Healthcare. **Data, code, and materials availability:** All data associated with this study are present in the paper or the Supplementary Materials. Mutant HIV-1 strains will be made available to researchers by contacting the corresponding authors.

Submitted 27 June 2025  
 Accepted 10 November 2025  
 Published 7 January 2026  
 10.1126/scitranslmed.aea0947